

# Estimation of the central-axis-reference percent depth dose in a water phantom using artificial intelligence

Fernando Patlan-Cardoso<sup>a</sup>, Suemi Rodríguez-Romo<sup>ID, a</sup>, Oscar Ibáñez-Orozco<sup>a</sup>, Katya Rodríguez-Vázquez<sup>b</sup> and Francisco Javier Vergara-Martínez<sup>c</sup>

<sup>a</sup>Centro de Investigaciones Teóricas., Facultad de Estudios Superiores Cuautitlán, Universidad Nacional Autónoma de México, Cuautitlán Izcalli, México; <sup>b</sup>Universidad Nacional Autónoma de México, Cuautitlán Izcalli, México; <sup>c</sup>Departamento de Metrología, Instituto Nacional de Investigaciones Nucleares, Cuautitlán Izcalli, Mexico

## ABSTRACT

The water phantom is used as a standard device for the calibration of measuring instruments used in radiation therapy. To carry out this calibration, it is essential to characterize the distribution of the percent depth dose (PDD) along the central reference axis, since this is where the instruments to be calibrated are located. The PDD depends on some magnitudes, such as the size of the field in the phantom, the depth of the central reference axis, the source-to-surface distance (SSD) and the radiation energy used [23]. A phantom is a fundamental element for the training of cancer specialists and medical physicists, and can be used to propose more effective procedures for the clinical radiation treatment of patients. We report on some models and simulation of the PDD data provided by the International Atomic Energy Agency (IAEA) and the British Journal of Radiology [1] by using artificial intelligence. PDD predictions by using artificial neural networks (ANN) and genetic programming (GP) are hereby given. It is shown how our approach has superior performance compared to the current state of the art.

## ARTICLE HISTORY

Received 8 May 2020  
Accepted 21 November 2020

## KEYWORDS

Radiation dosimetry;  
Calibration instruments;  
Percent depth dose; Artificial  
neural networks; Genetic  
programming

## 1. Introduction

The ionizing radiation equipment calibration is a critical task that requires not only knowledge, skills, techniques, and protocols, but also recommendations from organizations responsible for proper application of ionizing radiation in whole disciplines, such as those involved in therapeutic cancer treatment, which is our main interest in this paper. Accuracy and traceability of the measurement of the absorbed dose in the water of the radiotherapy beam is a critical factor in achieving a curative outcome in cancer patients, among others. There have been several attempts over decades to systematize such processes. The planning of treatments with Gamma and megavoltage X-ray beams must take into account the deep penetration of different materials. Dose absorbed in water is the variable that is used to calibrate ionizing radiation measurement instruments in radiotherapy treatment.

A radiotherapy phantom is a device designed to simulate the human body under the effect of ionizing radiation. Many different types of phantoms are used in therapy, classified depending on the radiation type and the target organ. In our case, we focus on a special type of phantom used in radiation therapy: the water phantom (Attix, 1991; Faiz & John, 2014). This phantom is filled with demineralized water.

Ionization chambers are one of the most widely used instruments in radiotherapy. An ionization chamber is a gas-type detector that converts radiation energy into electrical energy which can be quantified and processed by electronic measuring devices (Knoll, 2010; Price, 1964). Ionization chambers are calibrated according to the procedure described in the International Atomic Energy Agency (IAEA) code of practice 398 (Andreo et al., 2006). This code of practice states that standard instruments must be calibrated in a Primary Standard Dosimetry Laboratory (PSDL) so that they can then be referred to a Secondary Standard Dosimetry Laboratory (SSDL), which ultimately serves the user.

In the calibration process, there is one particular measure that is very important; the PDD which is widely used in the treatment planning that specialist physicians and other health professionals apply to a patient undergoing radiotherapy and it is defined as the relationship between the central reference axis absorbed dose and the maximum absorbed dose, expressed as a percentage.

Many parameters affect the PDD in the water phantom. These include beam quality, depth on the center axis ( $z$ ), field size area ( $A$ ) and field shape, source-to-surface distance (SSD), and collimation beam, which serves to homogenize the path of the source's

emissions leaving in all directions, thus producing a beam of rays with the same properties. PDD decreases with the depth (after the maximum dose depth is reached) and increases with the energy beam. There is a zone before the maximum dose depth is reached, where the minimum absorbed dose is precisely at the surface of the phantom (in the central axis) and the skin-sparing or skin preservation effect occurs, from there it increases as it approaches the maximum dose point. This phenomenon is known as the 'dose buildup' and produces a dose accumulation region.

The field size can be defined in two ways; geometrically and dosimetrically. From the geometrical point of view, it is defined as 'the projection, on a plane perpendicular to the beam axis, of the distal end of the collimator as seen from the front center of the source' (Faiz & John, 2014). From a dosimetric point of view, K.M. Faiz (Faiz & John, 2014) defines the field size as the distance intercepted by a given isodose curve (usually 50%) on a perpendicular plane to the beam axis at a given distance from the source. A 4 × 4 cm type cone collimator is used to calculate the PDD for Gamma and X-rays in the simulations reported here, since this is the standard experimental practice.

As for the phantom, the field size is given by a screen of pre-set dimensions, located at the center of the phantom that is directly exposed to the radiation beam. This screen can take different shapes, among which the square is the most common. Rectangular and even circular shapes are also used. An important aspect to consider in the phantom design is that the screen thickness must be very small, so that its contribution in experiments can be taken as insignificant.

It is possible to transform a field of any shape into an equivalent rectangular field (Attix, 1991; Faiz & John, 2014; Podgorsak, 2006). Therefore, according to the IAEA practice code 398, the calibration of the radiotherapy equipment is carried out only with an equivalent rectangular field size of 10 × 10 cm<sup>2</sup>. The reason for this is that the irradiation field sizes applied to oncological lesions are irregularly shaped, which is not convenient in terms of reference conditions when calibrating the radiation instruments.

Another important variable in the characterization of the phantom is the distance from the source of irradiation to the surface of the phantom; namely the surface-to-source distance (SSD). This is defined as the distance between the source of radiation and the front surface of the phantom in the center. See Figure 1 for further details.

PDD is a function of the field size area  $A$ , the depth at the center axis of the phantom  $z$ , the source-to-source distance SSD, and the energy of the radiation used. The focus of this paper is to characterize the

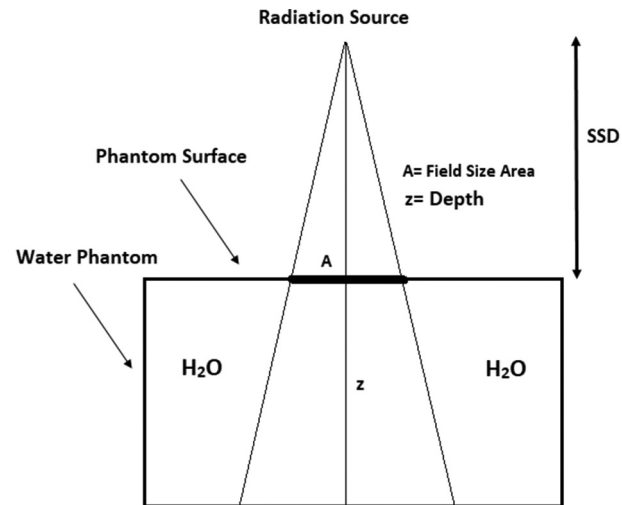


**Figure 1.** A two-dimensional projection of the water phantom for radiotherapy.

water phantom PDD values on its central axis of reference by providing these values via artificial intelligence (AI) models. There has been only one successful proposal for this PDD function reported so far due to the complexity of the radiation and water interactions effects over the phantom PDD behavior as  $z$ ,  $A$  and SSD changes. This is the following well-known empirical equation, called Pfalzner equation in this paper (Wood, 1974).

$$PDD(z, A, SSD) = \frac{k(z)}{k(z_{max})} \left( \frac{A}{SSD^2} \right)^{m(z)-m(z_{max})} \frac{(SSD + z_{max})^{2-2m(z_{max})}}{(SSD + z)^{2-2m(z)}}. \quad (1)$$

In equation (1);

- $z$  is the depth (cm).
- $A$  is the area of the irradiation field (cm<sup>2</sup>).
- SSD is the surface-to-source distance of the phantom (cm).

•  $z_{max}$  is the depth on the phantom central axis of reference, where the maximum-absorbed dose occurs (cm).

•  $k(z)$ ,  $k(z_{max})$ ,  $m(z)$  and  $m(z_{max})$  are empirical functions, outcome of PDD data fitting, that in the case of Co-60 beams, are as follows:

$$k(z)=$$

$$1.00778 - 0.063527z + 0.0014216z^2 - 0.0000z^3.$$

$$2 m(z)=0.0113 + 0.0070903z - 0.0000593z^2.$$

Equation(1), while it complies with the behavior of Cobalt-60 Gamma radiation within the phantom, it has an improvable margin of error calculated from the experimental data. In the case of X-rays, no analytic expression is available in the literature. Therefore, in most cases, the phantom is characterized experimentally to calibrate measurement instruments or to plan for some radiation therapy. Pfazlner equation and the equation proposed in this paper are empirical; thus, they are valid in (or sufficient close to) a solution space.

The experimental characterization of a phantom has the disadvantage that the invested time is quite large and does not allow us to predict the behavior of the same phantom in scenarios distant from the concerned experiments. This paper presents a way to model and simulate the phantom through the use of scientific computation. Once we have proven that we can reproduce the real experiment behavior, ensuring a minimal error, we are ready to efficiently predict the PDD values. Namely, we expect to predict the PDD behavior in a variety of cases where no experimental data is available. This is done by using powerful AI; artificial neural networks (ANNs) and genetic programming (GP).

Alternative approaches to the study and application of ionizing radiation, mostly via Monte Carlo methods (Apipunyasopon et al., 2013; Li et al., 2011; Mesbahi et al., 2006), have been successful throughout the ending of the XX century and the beginning of XXI century. Among others, let us mention Los Álamos National Laboratory where the MCNPX code (Sawakuchi et al., 2010; Zhang et al., 2006) was developed; the Organization for the Economic Cooperation and Development (OECD) where, in alliance with the University of Barcelona, the PENELOPE code (Penetration and Energy Loss of Positrons and Electrons) (Baumgartner et al., 2009; Panettieri et al., 2009; Ramirez et al., 2011) was introduced; and The European Organization for Nuclear Research (CERN), where the GEANT4 and ROOT code (Bakkali et al., 2016; Fleckenstein et al., 2013; Kandlakunta et al., 2019) were generated. Even though artificial intelligence was already known at that time (Wu & Zhu, 2000) in the field, it was an exotic computational tool, not well understood, and developed to be included in the original codes. Today the situation is different; however, it is usual that the AI tool-kits, for GEANT4 and ROOT as an example, incorporates the ANNs as a powerful work tool (Brun et al., 2018) on Monte Carlo premises. Here, we intend to pave the way to include AI methods from first principles and experimental data; nothing is taken for granted or assumed. Even more, right now, there are plenty of AI methods based on artificial neural networks and bio-inspired programming that can be used to better fit ionizing radiation models and experiments. These methods, besides allowing us to compare the output obtained with the Monte Carlo method, allow us to extend the solutions space to provide, as it is done in this paper, an empirical equation of the PDD as a function of z, A, and SSD for Gamma rays of Cobalt 60 based only on the hidden patterns in the experimental data.

ANN is a typical computational model of artificial intelligence based on the biological behavior of neurons (Freeman & Skapura, 1991), while genetic programming is a specific case of the use of genetic algorithms for problem-solving (Langdon & Poli,

2002). The code was splitting the data into two sets; the training and the test sets. The overall idea is to uncover the hidden patterns in the experimental data, learn from them, and predict new data based on these. While the training data are used to learn these patterns, the test data prove that we are producing a well-educated ANN capable of reproducing already known experimental data (from the test set), up to a fixed error. Once this is done, the code must be valid to produce data inside the solution space within (or at least close enough) the error margin. Artificial neural networks are interconnected elements that receive information, process it and produce output information in a very similar way as biological neurons do. They can easily be considered as weighted directed graphs. Each neuron (node) is interconnected with other neurons through weighted links. The number of layers or levels in the network determines its complexity. The topology of the artificial neuron network is given by the problem to be solved. ANNs have been very successful when used within the field of nuclear sciences. For example, Santos, et. al. (2012), and Vega-Carrillo, et. al. (2006) developed techniques for neutron spectrometry with a fairly good approximation. Medhat, M. E. (2012) and Yoshida, et.al. (2002) developed a technique to reconstruct the gamma-ray spectra of isotopes that had been detected using a hyperpure Germanium detector. On the other hand, Pilato, et. al. (1999) established a technique to perform radionuclide spectrometry through artificial neural networks. Thus, it is natural to consider that ANNs are an excellent option for modeling and simulating the PDD in a water phantom.

Genetic programming (a specialized branch of genetic algorithms) is a machine learning paradigm of evolutionary computing that serves to carry out a specific task. It is a special case of optimization where the user defines the heuristic, relies on the use of decision trees, and adjusts a population of programs according to an aptitude function or fitness which evaluates the ability of each program to perform the pre-determined task with the highest possible accuracy. As with ANNs, genetic programming also requires some parameters to achieve its goals (Langdon & Poli, 2002) among these parameters we can mention the population, the generations, and the optimization algorithm.

Although genetic programming has not been used as frequently as desired to solve nuclear science problems, so far, some exceptional examples are provided in references (Alamaniotis & Jevremovic, 2015; Kumar & Pavel, 2015; Pinheiro & Schirru, 2018) and (Pozzi & Segovia, 2000).

## 2. The model

The precision of the measurements delivered by the ionization chamber, as well as the radiation beam

output, are fundamental elements in the administration of precise doses in tumor lesions, which is part of the quality assurance of radiation therapy dosimetry. This is why it is very important to develop new techniques and tools that allow us to model the PDD in the central axes of reference in a water phantom, since this is widely applied, both in instrument calibration and treatment.

In this paper, we present a method to analyze Gamma-rays and X-rays of various energies for different field sizes. The method does not rely on separating the primary and scattered components and fitting the scattered component into a semi-empirical formula as it is done in references (Pal et al., 2002; Wood, 1974). Thus, we can see how at larger depths in the finite medium, the reduction in intensity due to absorption and due to the inverse square law becomes more dominant than the scattered contribution. All the percentage depth doses are normally expressed in terms of the depth of maximum dose.

The ANN and GP codes were created using the Phyton 3.6 programming language. The minimum hardware requirements to run the simulation are Intel Core i7, 2.5 GHz or higher microprocessor, 500 GB of free space or more to save created image files, 8 GB in RAM, LED FHD monitor and a graphics card for video accelerator. The estimated computing time for the PDD in-depth dose calculations in our model is approximately 7 hours.

This research is carried out for two different radiation sources; Cobalt 60 (Co-60) Gamma Rays and X-rays produced by a linear accelerator with an energy of 6 and 15 MV.

For Co-60 experiments, data come from the Code of Practice 398 worksheet published by IAEA. This worksheet presents PDD data for a phantom with a field size up to  $45 \times 45 \text{ cm}^2$ , although usually the reference phantom for instrument calibration is sized  $30 \times 30 \times 30 \text{ cm}^3$ . The data is available for various field sizes, including the  $10 \times 10 \text{ cm}^2$  field size, which is recommended by IAEA for equipment calibration used in radiation therapy. Phantoms are manufactured with high-quality PMMA (polymethylmethacrylate).

The Code of Practice 398 worksheet data published by IAEA is a compilation of results from different laboratories of the IAEA's network, secondary laboratories, and the International Bureau of Weights and Measures (BIMP) (IAEA, 2004). These data are the input of our ANN model with gradient-descendant training algorithm and genetic programming algorithm. In the ANNs, data from some phantom field sizes were used as training data, and the data from the remaining phantom field sizes were used to test the predictability of the network. In the case of the genetic programming algorithm, all available PDD experimental data for different field sizes were used

as inputs to generate an equation that gives a minimum error to predict the IAEA data.

The artificial neural network (ANN) presented in this paper for Co-60 has the following topology. Four hidden layers; the first with 200 neurons, and the remaining three with 100 neurons each. We use 2,000,000 epochs and a training rate of 0.354050603 for a descending gradient algorithm. Our ANN has three inputs and one output; the inputs are z, A, and SSD, the output is the PDD. The activation function is of the sigmoid type. The training was performed for field sizes  $10 \times 10 \text{ cm}^2$ ,  $15 \times 15 \text{ cm}^2$ , and  $20 \times 20 \text{ cm}^2$ . These field sizes are chosen to create a range for the ANN study that allows predicted cases which can be used for different applications. For predictions beyond this range, new training data should be provided in order to solve the concerned matter.

In this paper, we show a method to predict PDD in any field size (Das et al., 2007). Thus, we reproduce with minimum error the Co-60 PDD curves for phantom field sizes  $10 \times 10 \text{ cm}^2$ ,  $15 \times 15 \text{ cm}^2$ , and  $20 \times 20 \text{ cm}^2$ . Once the ANN model reproduces well known PDD data, it is used to predict intermediate field sizes, such as  $12 \times 12 \text{ cm}^2$ ,  $14 \times 14 \text{ cm}^2$ ,  $16 \times 16 \text{ cm}^2$  and  $18 \times 18 \text{ cm}^2$ . Traditional radiotherapy techniques use field sizes of the order of  $4 \times 4 \text{ cm}^2$  to  $40 \times 40 \text{ cm}^2$ , this is the reason to generate phantom databases with field sizes in this range. As a first approach, we compare these predictions with the data produced by the Pfalzner equation (Wood, 1974).

In the case of the equation generated by the GP algorithm, data from all field sizes are used. A population size of 20,000 individuals with 600 generations and fitness of 0.628376 provides an accurate equation. Thus, the results obtained by this equation were compared with those produced by the Pfalzner equation and data from IAEA experimental experiments.

In the case of X-rays, we obtain the data from reference (Hamed Abd El-Kader, 2014). Here, the authors show that the experiments published by the British Journal of Radiology in 1996 (Aird, 1996), are correct. To do so, they reproduce the very same experiments for different settings, for instance; a Linear Accelerator (LINAC) Elektra Precise, a water phantom with dimensions  $30 \times 35 \times 30 \text{ cm}^3$  manufactured with PMMA, a  $0.125 \text{ cm}^3$  and  $0.6 \text{ cm}^3$  Farmer dual ionization chamber and a PTW-UNITED electrometer (see Figure 2) for SSD of 100 cm. The error measurement is quite small. The minimum and maximum standard deviations were  $\pm 0.09$  and  $\pm 0.11$  for 6 MV and  $\pm 0.08$  and  $\pm 0.12$  for 15 MV, which comply with the published recommended tolerance (Aird, 1996). The experiments were performed for energies 6 MV and 15 MV.

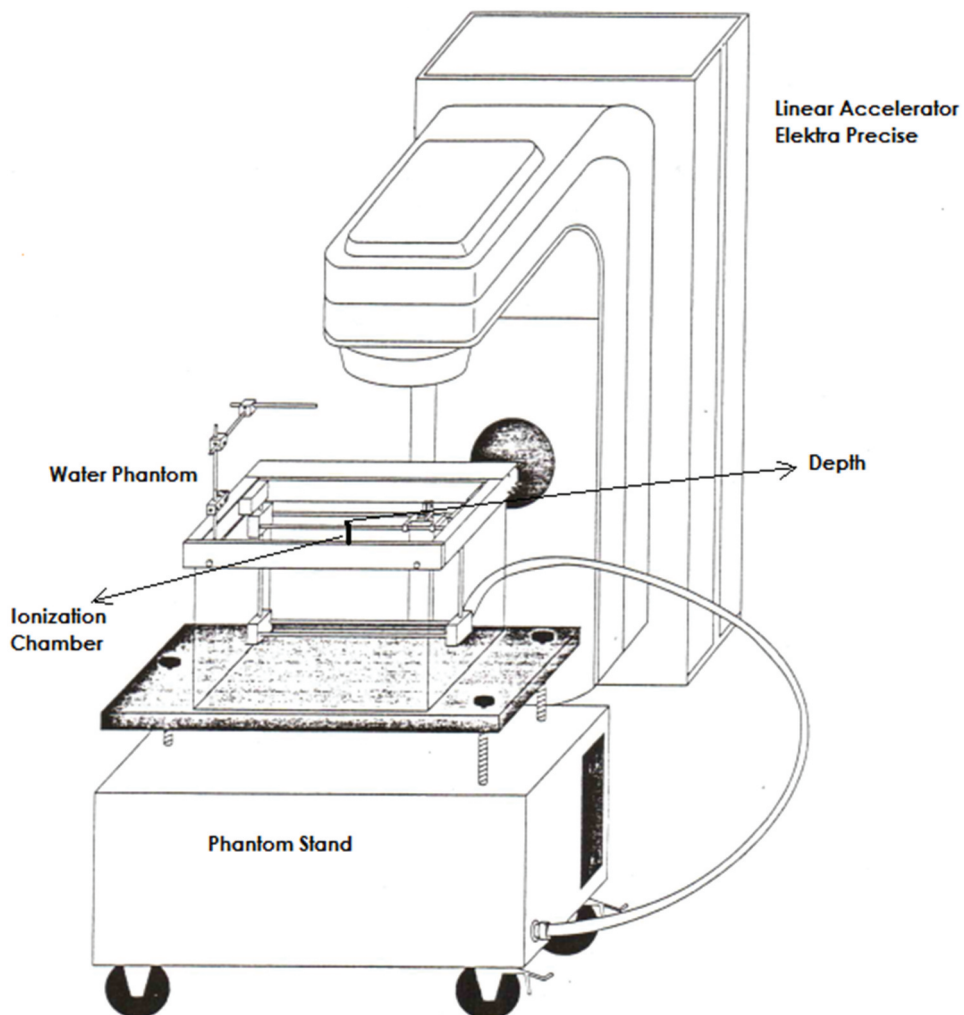


**Figure 2.** Experimental setting used to measure the PDD in a water phantom with a linear accelerator (LINAC).

Similarly to what was done for Co-60, in the case of X-rays an ANN was designed to reproduce 6 MV and 15 MV X-rays, producing PDD data for standard field sizes; then, the proposed ANN model is used to predict PDD data of uncommon but useful field sizes. Here, the gradient-descendant algorithm was used, the depth on the phantom central axis, the field size, and the SSD of the phantom are taken as inputs. The output, as expected, is the predicted PDD on the central axis of the phantom. Thus, PDD is taken as a function of three variables;  $z$ ,  $A$ , and SSD for a fixed energy (either 6 MV or 15 MV). This is enough to reproduce, via ANN, all experiments plus any imputed data in the solution space. For further purposes, for instance, to propose a new equation via genetic programming, we shall not set the energy as a parameter like we do in this manuscript. This shall be reported elsewhere.

The topology of the ANN used is as follows: three inputs, one output, and four hidden layers. The inputs are  $z$ ,  $A$ , and the SSD. One ANN is generated for each energy of the X-ray beam, in this paper 6 and 15 MV. The ANN model for X-rays was designed with four hidden layers, 100 neurons per layer and 20,000,000 epochs. Again, the activation function is of the sigmoid

type. The training was performed for field sizes of  $5 \times 5 \text{ cm}^2$ ,  $15 \times 15 \text{ cm}^2$  and  $30 \times 30 \text{ cm}^2$ . Predictions are made for different field sizes;  $10 \times 10 \text{ cm}^2$  and  $20 \times 20 \text{ cm}^2$ . The training was performed for both 6 MV X-rays and 15 MV X-rays.

### 3. The artificial intelligence program

The International Commission on Radiation Units and Measurements (ICRU) report-24 (1976) recommended at least an accuracy of  $\pm 5\%$  in the delivery of absorbed dose to the target volume of the treated tumor. The precision accuracy value in a dose administration is  $\pm 3.5\%$  at one standard deviation level as per Brahme (1984) and  $\pm 3\%$  as per Mijnheer et al. (1987) to reduce the acceptable complication of tissue in risk. The accuracy limit described above includes the measurement of the absorbed dose, the acquisition of patient data, the treatment planning, and the execution of the prescribed dose planning for the tumor. This implies that the accuracy of each stage of the measurement process must be better than the tolerance value established in the therapy protocols to achieve the curative

outcome of the treatment. Hence, the quality assurance program has an increasingly important role in radiotherapy technology. Absorbed-dose-to-water calibrations are important for the medical community in order to facilitate the accurate dose delivery to tumors during external-beam cancer therapy (Reza et al., 2018).

Two algorithms were codified and implemented to reproduce the central-axis percent depth dose induced by a (Gamma or X) radiation beam over a water phantom, which simulates human tissue. See Figure 3, in part (a) the flowchart for the ANNs used is presented and in part (b) the flowchart to obtain the GP equation. In this section, we comply with the standards of scientific computing (Freeman & Skapura, 1991; Langdon & Poli, 2002). The corresponding pseudocodes are the following.

- Artificial Neural Network:

```
BEGIN/*Artificial Neural Network*/
```

Generate an input vector at the input nodes.

```
FOR/*Weight Activation*/
```

The inputs and weights are used to decide whether the output neurons are activated or not.

```
BEGIN/*Error calculation*/
```

The error is calculated as the difference between the outputs of the network and the planned target values.

```
IF/*Error evaluation*/
```

If the error is not adequate, return to the activation of weights.

```
IF Error is appropriate THEN
```

Finished: = TRUE

```
END
```

```
END
```

- Genetic programming:

```
BEGIN/*Genetic Programming Algorithm*/
```

Generate an initial population.

Calculate the evaluation function of each individual.

```
WHILE NOT Finished DO
```

```
BEGIN/*Produce a new generation*/
```

```
FOR/* Population size */DO
```

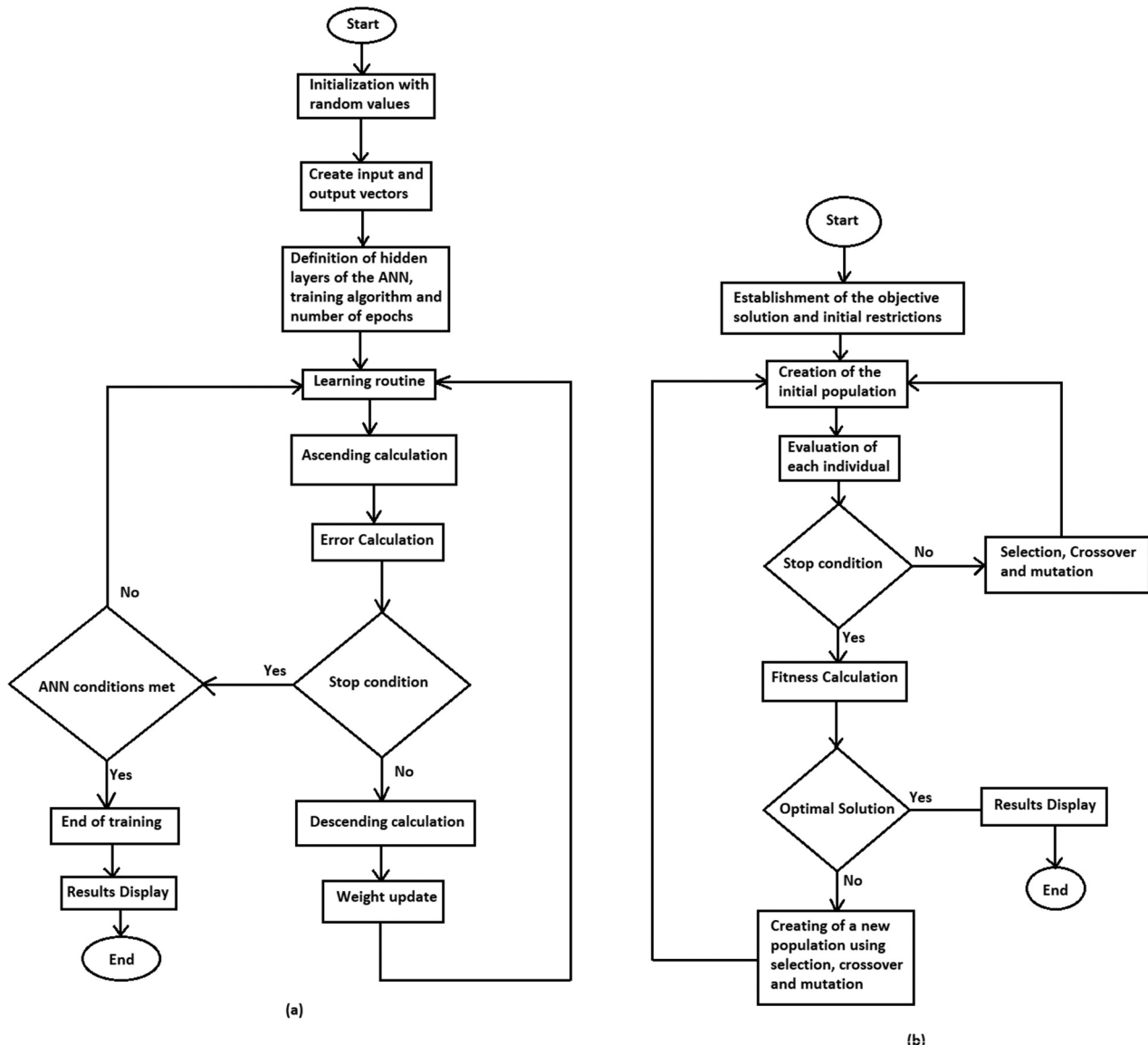


Figure 3. Flowchart for the(a) ANN model and (b) the GP equation.

BEGIN/\*Reproductive cycle\*/

Select the individuals of the previous generation for the crossing. The probability of selection is proportional to the evaluation function of the individual. Cross with some probability the two individuals obtaining two descendants. Mutate the two descendants with some probability. Calculate the evaluation function of the two mutated offsprings. Insert the two mutated descendants in the new generation.

END

IF the population has converged THEN

Finished: = TRUE

END

END

#### 4. The results

Firstly, we present the results of the PDD produced by the ANN model applied to the Co-60 case. This is done for each of the different phantom field sizes. Then we compare the output with both; the data provided by the Pfalzner equation (Wood, 1974) and the experimental data provided by the IAEA. Subsequently, the analysis for the X-rays generated by the LINAC Elektra Precise is presented. The analysis is performed for different field sizes.

##### 4.1. Gamma rays, Co-60

For Co-60 Gamma rays, IAEA reports data for different field sizes (IAEA, 2004). These data correspond to depths of 0.5 cm to 30 cm (with increments of 0.1 cm) on the central axis of the phantom, up to

30 cm depth. All the IAEA experimental values used in the ANN model and the GP equation to simulate the Co-60 PDD are depicted in Figure 4. Please, recall that these data are taken for a fixed SSD of 100 cm.

With the experimental values of the IAEA, an equation was constructed using genetic programming which produces better results than Pfalzner equation. This equation is as follows:

$$PDD = \frac{-107.735 + 3.401z^{-1} + (z - 0.737)\sqrt{\frac{3.096z+A+SSD}{z+0.679A}}}{\sqrt{e^z \sqrt{\frac{1}{3.356A+SSD}}}}. \quad (2)$$

Here, z, PDD, and A are defined as in equation (1). This equation in the subsequent is called the GP equation since this was fully generated by genetic programming from the coarse IAEA experimental data.

The numbers that appear in equation 2 are the result of the optimized genetic programming. We start with a set of 'genes' or simple programs. Then, the experimental data and the mathematical operations are selected, crossed, and mutated, as it is done in nature, producing new generations and individuals who replace the previous ones. After a certain number of generations, the optimal equation is obtained, and the numbers in this are the result of the replacement, selection, crossing, and mutation of the experimental data and the original mathematical operations or genes.

We remark that equation 2 is suited only for Gamma rays of Co-60. The hidden patterns, leading to equation 2, are produced by the corresponding experimental data; namely, it is an empirical equation. The different energies for X-rays and Gamma rays lead to different

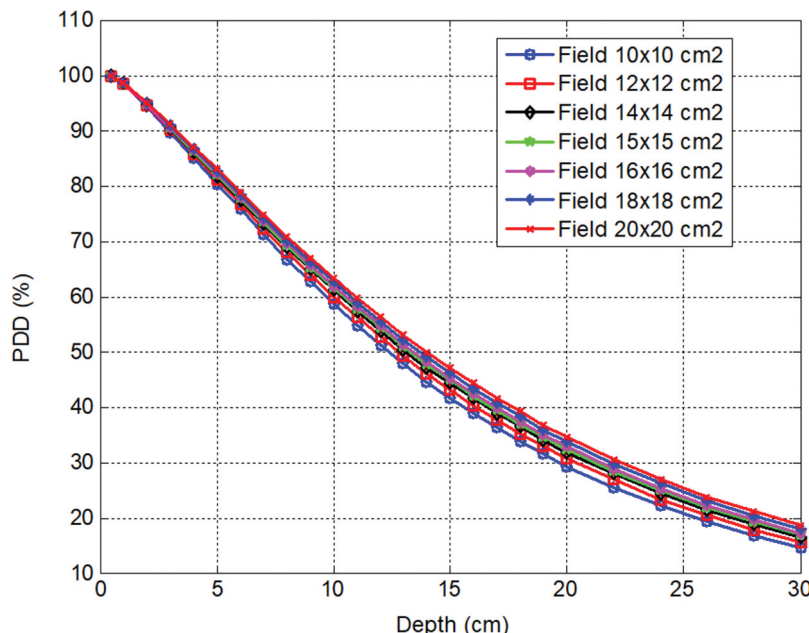


**Figure 4.** The PDD from the IAEA experimental data-set for the field sizes;  $10 \times 10 \text{ cm}^2$ ,  $15 \times 15 \text{ cm}^2$ ,  $20 \times 20 \text{ cm}^2$ ,  $12 \times 12 \text{ cm}^2$ ,  $14 \times 14 \text{ cm}^2$ ,  $16 \times 16 \text{ cm}^2$  and  $18 \times 18 \text{ cm}^2$ . The PDDs from the first three field sizes are used in this paper to train the ANNs implemented, and the PDD data for the remaining field sizes are used to verify our ANN model prediction. All IAEA experimental data were used to find the equation (2) by genetic programming.

PDD maximums when we consider PDD as a function of  $z$ ; actually both functions (one for X-rays and another for Co-60) shall be different. We are currently working on finding an equation for the PDD in X-rays of 6 and 15 MV, this shall be reported in the near future.

In Figure 5, all PDD values are normalized by the IAEA experimental data. Here we present the normalized PDDs predicted by the ANN model, the equation (1), and the equation (2), for different field sizes. The average relative error (AVRE) of the simulated PDDs for the ANN model and the equations (1) and (2) are given in Table 1. From this, we conclude that the ANN model produces much better results than the well-known Pfalzner equation (1). On the other hand, generally speaking, we observe that the GP equation presents a better behavior than the Pfalzner equation. We are positive to assert that the ANN models and GP equation are adequate to predict PDD data for uncommon field sizes. Besides the GP method provides with an equation for Gamma rays of Co-60 which is a very useful tool in most applications (2019).

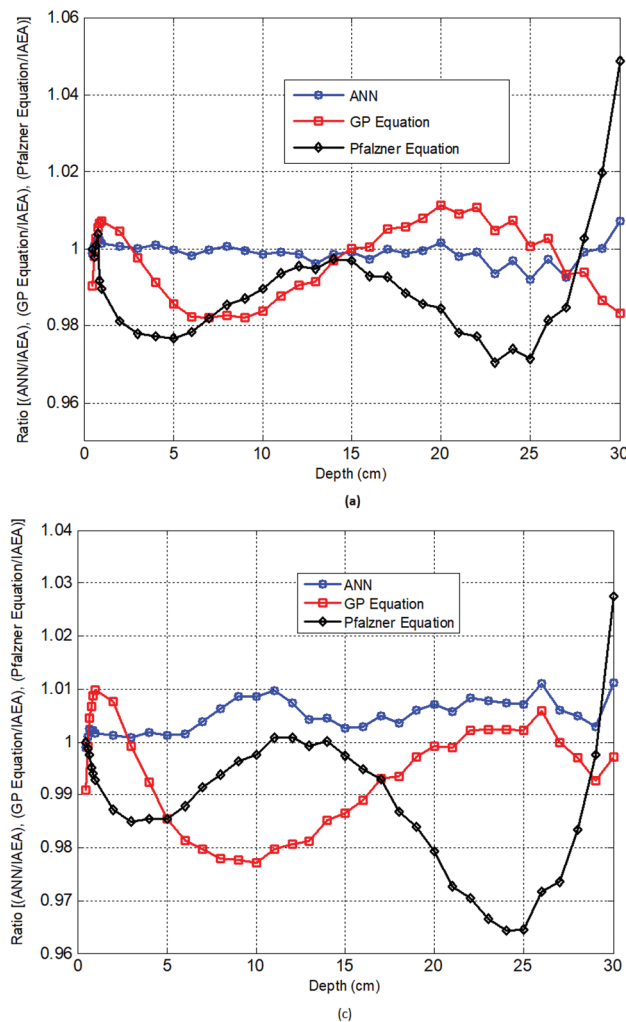


**Figure 5.** Normalized (by the IAEA experimental data) PDD given by the ANN model, the Pfalzner equation ((1)) and the GP equation ((2)). These data are provided for field sizes; (a)  $10 \times 10 \text{ cm}^2$ , (b)  $12 \times 12 \text{ cm}^2$ , (c)  $18 \times 18 \text{ cm}^2$ , (d)  $20 \times 20 \text{ cm}^2$ .

Note that all the models we are dealing with have an accuracy acceptable for nowadays practitioners. However, in this paper we are proposing a better code of practices for safer radiotherapies, at least as far as the improvements in calibration allow.

#### 4.2. X Rays, 6 MV

For X Rays in general, and 6 MV energy in particular, only the ANN predictions are considered in this paper. The ANN model hereby proposed involves a gradient-descendant algorithm, three inputs one output, and four hidden layers with 100 neurons each. The field sizes used for training are;  $5 \times 5 \text{ cm}^2$ ,  $15 \times 15 \text{ cm}^2$ , and  $30 \times 30 \text{ cm}^2$ , and for prediction;  $10 \times 10 \text{ cm}^2$  and  $20 \times 20 \text{ cm}^2$ . Recall that for X-rays no empirical or semi-empirical equation for PDD is available. Figure 6 shows the experimental data for the different field sizes used. Figure 7 shows the PDD values, normalized by the British Journal of Radiology (Aird, 1996), predicted by the ANN model.

Table 2 shows the AVRE for each of the field sizes used. As we do for Co-60 Gamma rays, we also

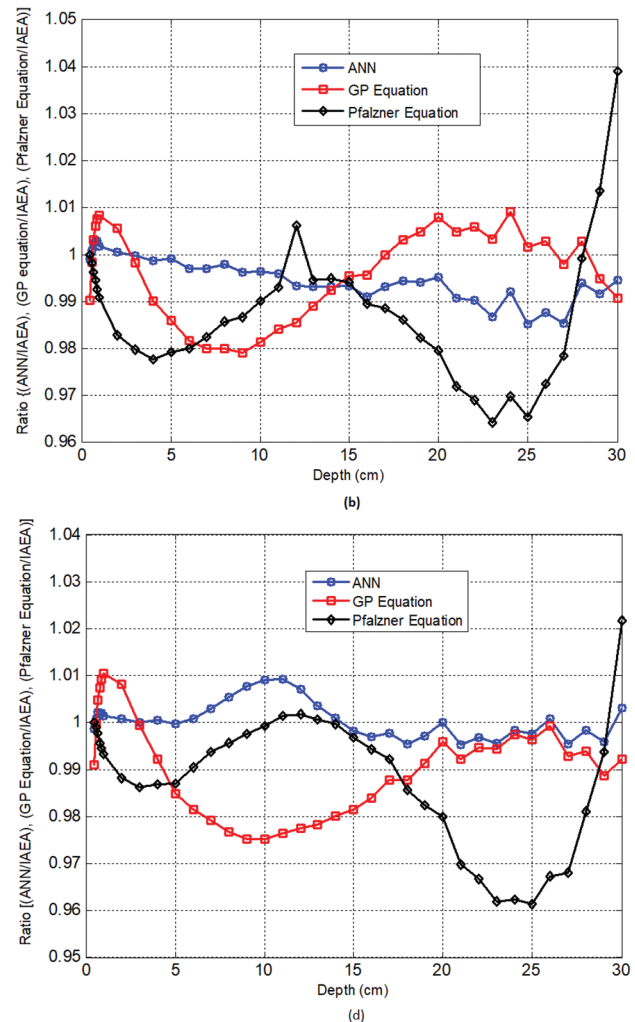


**Table 1.** The average relative errors (AVRE) for the PDD values simulated in the ANN model, the Pfalzner equation (1) and the GP equation (2) for different field sizes.

Field size	ANN	GP equation	Pfalzner equation
10 × 10 cm <sup>2</sup>	0.20 ± 0.17	0.88 ± 0.55	1.55 ± 0.86
12×12 cm <sup>2</sup>	0.63 ± 0.37	0.85 ± 0.63	1.72 ± 0.92
14×14 cm <sup>2</sup>	0.30 ± 0.23	0.91 ± 0.67	1.63 ± 0.95
15×15 cm <sup>2</sup>	0.21 ± 0.19	0.97 ± 0.74	1.69 ± 1.005
16×16 cm <sup>2</sup>	0.24 ± 0.18	0.97 ± 0.73	1.57 ± 1.05
18×18 cm <sup>2</sup>	0.49 ± 0.26	0.99 ± 0.83	1.41 ± 1.12
20×20 cm <sup>2</sup>	0.30 ± 0.24	1.25 ± 0.77	1.44 ± 1.25

calculate the AVRE and RMS error corresponding to the different field sizes that are used, finding that for the case of the AVRE, this changes from 0.12 to 2.62, the RMS vary from 0.0007 to 0.018, which is quite acceptable.

As can be seen in Figure 7, as well as in Table 2, the result produced by the ANN model fits fairly well into the experimental data, being an accurate approach in agreement with references (Brahme, 1984; Mijnheer et al., 1987) and (Reza et al., 2018).

#### 4.3. X Rays, 15 MV

In this case, the PDD data from the field sizes used for training are 5 × 5 cm<sup>2</sup>, 15 × 15 cm<sup>2</sup>, and 30 × 30 cm<sup>2</sup>. For prediction, we use the PDD data for field sizes of 10 × 10 cm<sup>2</sup> and 20 × 20 cm<sup>2</sup>. The ANN training algorithm was again gradient descending with the model features described above for 6 MV of energy.

Figure 8 shows the experimental data for different field sizes used to test our ANN model. Figure 9 shows PDD predicted by our ANN model, all data are normalized by the experimental data.

The ANN model hereby introduced fits experimental data fairly well, which is reflected in the results shown in Table 3. The percentage of relative error is not larger than 1.5%; therefore, the performance of the ANN model can be considered suitable to model PDD for a water phantom in the central axis of reference when it is irradiated by X-rays of two different energies; 6 MV and 15 MV.

#### 5. Discussion and conclusions

Radiotherapy aims to deliver a uniform dose of radiation to a lesion of interest, sparing the normal healthy tissues surrounding this. For external-beam radiotherapy, data on the central axis percentage depth dose distributions and off-axis ratios for as many field sizes as possible, are needed. Furthermore, field sizes depend on the size and shape of the treatment sites; however, it is not practical to test any field size that can be encountered in the normal course of radiotherapy. Therefore, empirical formulations (for example, Pfalzner equation) to predict PDD must be used, usually excluding the buildup zone. In this paper, we propose an alternative approach via AI.

The methods and models introduced in this paper allow us to process data in two different ways, both thanks to AI; ANN and GP genetic. As can be seen in the results obtained, an ANN is a powerful tool to obtain the PDD in the central axis of a water phantom. On the other hand, we showed that through genetic programming it is feasible to find mathematical equations that allow us to characterize the PDD in the central axis of reference with quite a good approximation to experimental data, usually better than empirical equations

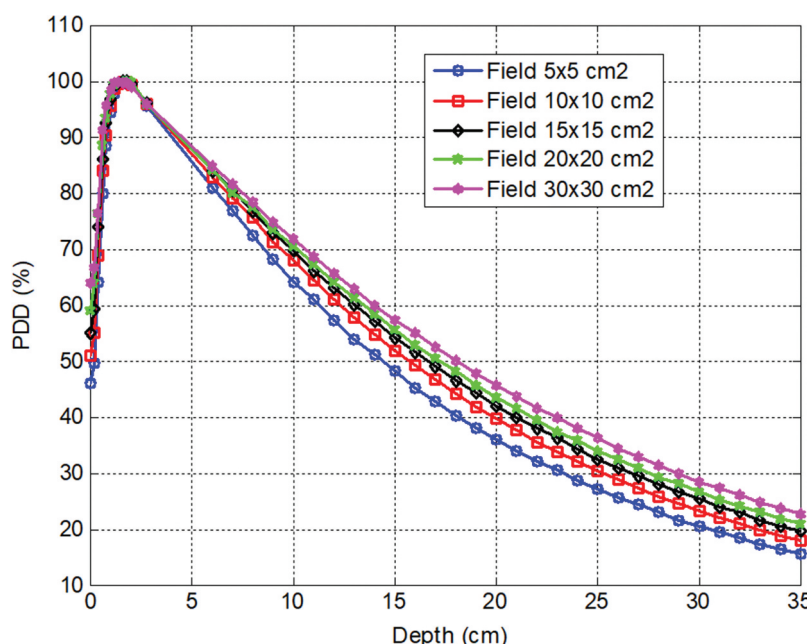


**Figure 6.** British journal of radiology (Hamed Abd El-Kader, 2014), PDD experimental data for field sizes; 5 × 5 cm<sup>2</sup>, 10 × 10 cm<sup>2</sup>, 15 × 15 cm<sup>2</sup>, 20 × 20 cm<sup>2</sup> and 30 × 30 cm<sup>2</sup>. X Rays, 6 MV.

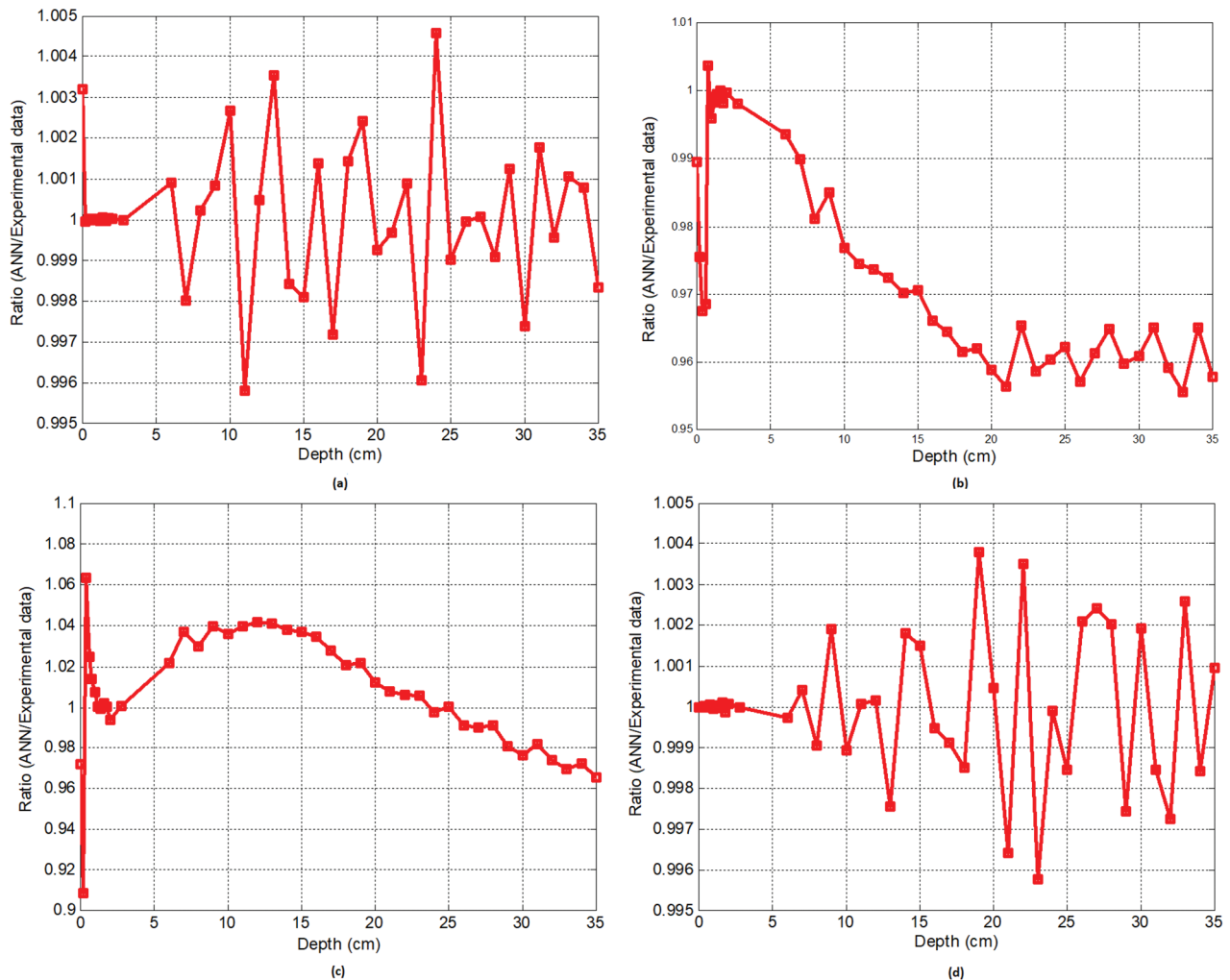


**Figure 7.** Normalized (by the experimental data) PDD predicted by the ANN model, for X rays and 6 MV of energy. Field sizes; (a)  $5 \times 5 \text{ cm}^2$ , (b)  $10 \times 10 \text{ cm}^2$ , (c)  $20 \times 20 \text{ cm}^2$  and (d)  $30 \times 30 \text{ cm}^2$ .

**Table 2.** AVRE for the PDD data simulated by the ANN model, X-rays, 6 MV of energy.

Field size	ANN Average relative error
$5 \times 5 \text{ cm}^2$	$0.12 \pm 0.12$
$10 \times 10 \text{ cm}^2$	$2.62 \pm 1.49$
$15 \times 15 \text{ cm}^2$	$0.12 \pm 0.14$
$20 \times 20 \text{ cm}^2$	$2.25 \pm 1.84$
$30 \times 30 \text{ cm}^2$	$0.12 \pm 0.12$

such as Pfalzner (Aird, 1996). The results obtained reflect (for both, the ANN and the GP approaches) errors that are within acceptable values and reproduce fairly well the experimental data. This has a positive impact on the conditions in which the characterization data of a water phantom is obtained since the time spent in this activity is quite high and the facilities used (either medical or due to primary and secondary dosimetric laboratories) cannot be employed for simultaneous radiotherapy service or calibration purposes, impacting in their optimal performance.

On the other hand, a very important aspect that we should not lose sight is that knowing the PDD, it is feasible to prepare in advance some specific

radiotherapy treatments for patients who require this, as well as the training of radiotherapy equipment operators. This implies that this work contributes not only to optimize the resources of the facility that works with a phantom but to the therapy of patients undergoing radiotherapy.

Since controlling accuracy is vital in radiotherapy calibration, we analyze in-depth the errors produced by ANN, Pfalzner and GP equations to reproduce experimental data. AVRE and root-mean-square (RMS) errors are calculated for the phantom and equal-sized sections within this, excluding the buildup zone.

We conclude that for the Gamma rays our approach produces the following output;

a) For  $10 \times 10 \text{ cm}^2$  field size, the whole phantom, namely PDD data from 0.5 cm (to exclude the buildup zone inside the phantom) to 30 cm from the source; the ANN RMS and AVRE are very small compared to the predictions of the GP and Pfalzner equations, actually this is the case for all field sizes.

b) The GP AVRE and RMS error are smaller than the Pfalzner ones; however, as the area of the field size increases, the AVRE and RMS error of the GP equation

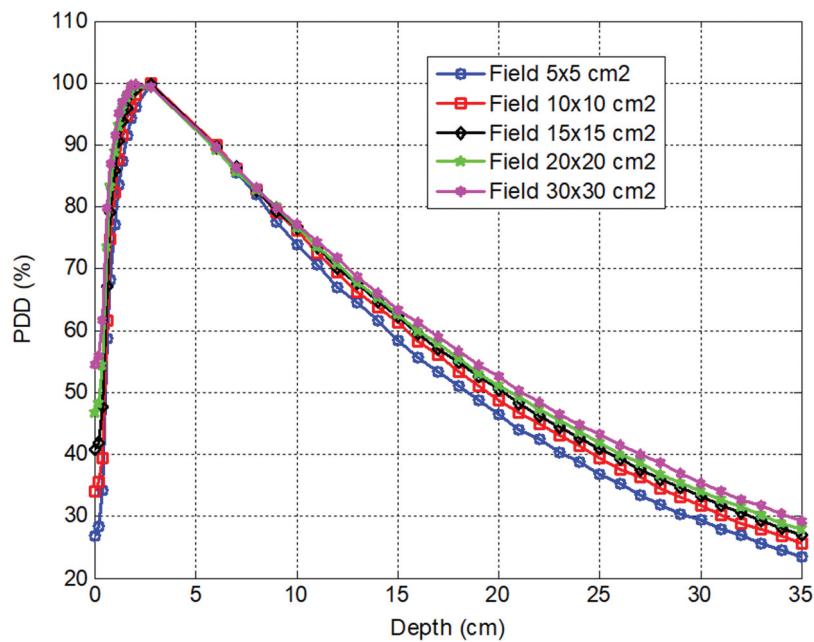


**Figure 8.** British journal of radiology (Hamed Abd El-Kader, 2014), PDD experimental for field sizes;  $5 \times 5 \text{ cm}^2$ ,  $10 \times 10 \text{ cm}^2$ ,  $15 \times 15 \text{ cm}^2$ ,  $20 \times 20 \text{ cm}^2$  and  $30 \times 30 \text{ cm}^2$ . X rays, 15 MV of energy.

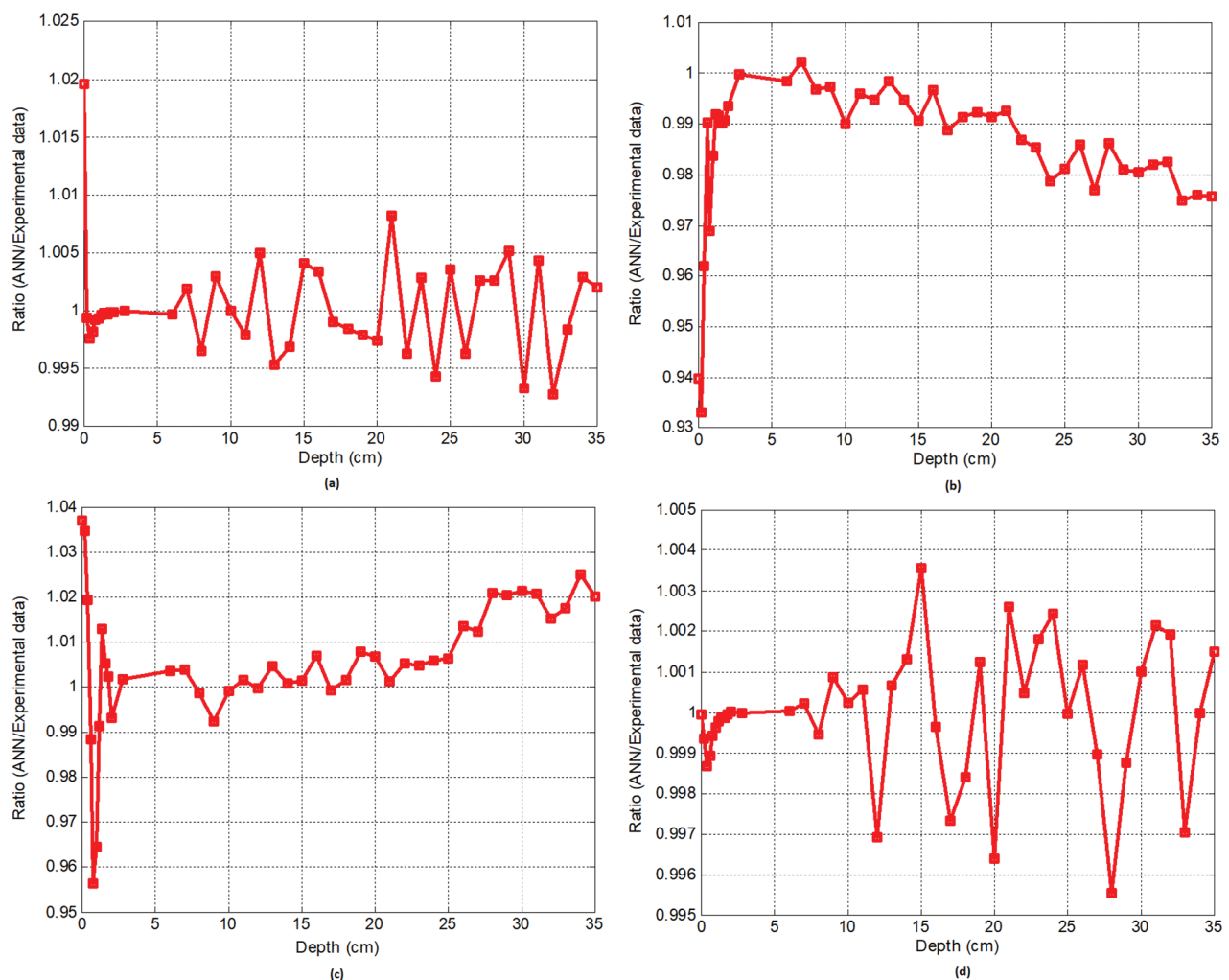


**Figure 9.** Normalized (by the experimental data) PDD predicted by the ANN model, for X rays and 15 MV of energy. Field sizes; (a)  $5 \times 5 \text{ cm}^2$ , (b)  $10 \times 10 \text{ cm}^2$ , (c)  $20 \times 20 \text{ cm}^2$ , (d)  $30 \times 30 \text{ cm}^2$ .

**Table 3.** AVRE for the PDD predicted by the ANN model, X-rays, 15 MV of energy.

Field size	ANN average relative error
5 × 5 cm <sup>2</sup>	0.30 ± 0.32
10×10 cm <sup>2</sup>	1.48 ± 1.37
15×15 cm <sup>2</sup>	0.13 ± 0.12
20×20 cm <sup>2</sup>	1.14 ± 1.10
30×30 cm <sup>2</sup>	0.11 ± 0.11

rise while the Pfalzner equation AVRE and RMS errors decrease, being the 15 × 15 cm<sup>2</sup> field size for AVRE and 16 × 16 cm<sup>2</sup> field size for RMS, the turning point, from there on, always Pfalzner equation AVRE and RMS error are smaller than GP equation AVRE and RMS errors.

c) For the PDD simulated data, from 0.5 cm to 30 cm, the ANN RMS error varies from 0.008 to 0.25 and the AVRE varies from 0.20 to 0.63, excellent for computational simulation. In the case of the GP equation, the RMS error ranges from 0.61 to 0.91 and the AVRE from 0.65 to 1.25, which is quite acceptable. For the Pfalzner equation, the RMS error varies from 0.69 to 0.91 and the AVRE from 1.42 to 1.72. This shows that the models introduced in this paper are the smart choice to fit Co-60 Gamma-rays from IAEA experimental data and achieve adequate predictions.

d) For the first third of the phantom (closer to the radioactive source), from 0.5 cm (to exclude the buildup zone) to 10 cm, we find that the behavior described in the last paragraph is replicated. In this case, the RMS error of the PDD simulated by the ANN model varies from 0.008 to 0.28, in the case of the GP equation the values range between 0.98 and 1.58, while for the Pfalzner equation these values are between 0.81 and 1.48. The values of AVRE are between 0.08 and 0.31 for the ANN, from 1.23 to 1.50 for the GP equation and from 0.99 to 1.75 for the Pfalzner equation. ANN and GP equation models remain competitive.

e) For the second third of the phantom (from 10.1 to 20 cm), the RMS error and AVRE for the simulated PDD values via ANN is smaller than the corresponding to the GP Equation and the Pfalzner equation. However, in this case the AVRE and RMS of the Pfalzner equation is always smaller than that of the GP equation, regardless of the size of the field being handled. The PDD simulated dates by ANN have an RMS that ranges from 0.09 to 0.27, for the GP equation varies from 0.38 to 0.95, while for the Pfalzner equation ranges from 0.33 to 0.44. As we can see, the ANN model still has the lowest error and the Pfalzner equation has a lower error than the GP equation. The AVRE of the PDD simulated by ANN is in between 0.17 and 0.67, for the GP equation in between 0.66 and 1.71 and in between 0.62 and 1.02 for the Pfalzner equation.

f) For the last third, namely from 20.1 to 30.0 cm, our ANN and GP equation models always provide an AVRE and RMS error smaller than the Pfalzner equation, regardless of the size of the field being handled. This indicates that in this region of the phantom, our models are a better option. The RMS errors handled by the ANN model vary from 0.07 to 0.23, those from the GP equation from 0.10 to 0.18 and those from the Pfalzner equation from 0.49 to 0.82, The AVRE of the produced data ranges from 0.25 to 1,008 for the ANN model, from 0.28 to 0.76 for the GP equation and from 2.14 to 2.83 for the Pfalzner equation.

For the X-rays, as was done for the Co-60 Gamma rays, the AVRE and RMS errors are analyzed. In these cases the first ranges from 0.001 to 1.14 and the second varies from 0.00085 to 0.0096, which indicates that simulations with ANN models are fairly reliable. The experimental data for 6 and 15 MV of X-rays matches well with our model under a certain limit.

As a reference to our work, we can mention the already reported study of measurement instruments. Even though PDD for instrument calibration, and PDD for radiation monitors (actually any measurement instrument) are not directly comparable, see for example, dErrico et. al (dErrico et al., 2001). In this reference the authors measure the energy of photoneutrons produced by a 6 and 18 MV X-ray equipment for personal protection dosimeters. Due to the characteristic of the instrument, the dosimetric magnitude is the equivalent dose, which assesses the damage produced in living tissue by ionizing radiation. In our paper we aim to obtain the PDD absorbed dose in water (inside a water phantom) for instrument calibration; a rather different goal. However, in Figure 3, by dErrico (dErrico et al., 2001), we can see the behavior of the equivalent dose for a 15 MV beam in a water phantom for a field size of 10 × 10 cm<sup>2</sup>. If we convert absorbed dose to equivalent dose through the quality factors established for the type of radiation being handled, we would observe that the values obtained by our model are very close to the values reported in that figure, since the maximum PDD is recorded near the surface of the phantom.

In this paper, we show how the PDD data from Co60 Gamma rays and X-rays of two different energies (6 MV and 15 MV) can be predicted. Even more, we show how ANN is always (for any field size and distance to the source) the smarter choice to fit experimental data with excellent predictability.

## Acknowledgments

We thank DGAPA-UNAM (PAPIIT-IT102920) and FESC-UNAM (PIAPI-1839) for partial support. FPC is grateful to CONACYT, Mexico for support.



## Disclosure statement

No potential conflict of interest was reported by the authors.

## Funding

This work was supported by the Dirección General de Asuntos del Personal Académico, Universidad Nacional Autónoma de México [PAPIIT-IT102920]; Consejo Nacional de Ciencia y Tecnología(MX) [N/A].

## ORCID

Suemi Rodríguez-Romo <http://orcid.org/0000-0002-3596-8535>

## References

- Aird, E. (1996). *Central axis depth dose data for use in radiotherapy 1996: A survey of this supplement depth doses and related data measured in water or equivalent media* (Vol. 25). British Institute of Radiology.
- Alamaniotis, M., & Jevremovic, T. (2015). Hybrid fuzzy-genetic approach integrating peak identification and spectrum fitting for complex gamma-ray spectra analysis. *IEEE Transactions on Nuclear Science*, 62(3), 1262–1277. <https://doi.org/10.1109/TNS.2015.2432098>
- Andreou, P., Burns, D. T., Hohlfeld, K., Bundesanstalt, P.-T., Huq, M. S., Kanai, T., Laitano, F., Smyth, V., & Vynckier, S. (2006). *An international code of practice for dosimetry based on standards of absorbed dose to water*. International Atomic Energy Agency.
- Apipunyasopon, L., Srisatit, S., & Phaisangittisakul, N. (2013). An investigation of the depth dose in the build-up region, and surface dose for a 6-mv therapeutic photon beam: Monte Carlo simulation and measurements. *Journal of Radiation Research*, 54(2), 374–382. <https://doi.org/10.1093/jrr/rrs097>
- Attix, F. H. (1991). *Introduction to radiological physics and radiation dosimetry* (1st ed.). Wiley-VCH.
- Bakkali, J. E., Bardouni, T. E., Safavi, S., Mohammed, M., & Saeed, M. (2016). Behaviors of the percentage depth dose curves along the beam axis of a phantom filled with different clinical to objects, a montecarlo geant4 study. *Radiation Physics and Chemistry*, 125, 199–204. <http://dx.doi.org/10.1016/j.radphyschem.2016.04.013>
- Baumgartner, A., Steurer, A., & Maringer, F. J. (2009). Simulation of photon energy spectra from varian 2100c and 2300c/d linacs: Simplified estimates with penelope monte carlo models. *Applied Radiation and Isotopes*, 67(11), 2007–2012. <https://doi.org/10.1016/j.apradiso.2009.07.010>
- Brahme, A. (1984). Dosimetric precision requirements in radiation therapy. *Acta Radiologica: Oncology*, 23(5), 379–391. <https://doi.org/10.3109/02841868409136037>
- Brun, R., Rademakers, F., Panacek, S., Antcheva, I., & Buskulic, D. (2018). *The ROOT Users Guide*. European Center for Nuclear Research (CERN).
- Das, I. J., Ding, G. X., & Ahnesjö, A. (2007). Small fields: Nonequilibrium radiation dosimetry. *Medical Physics*, 35 (1), 206–215. <https://doi.org/10.1118/1.2815356>
- d'Errico, F., Luszik-Bhadra, M., Nath, R., Siebert B.R., Wolf, U. (2001). Depth dose-equivalent and effective energies of photo neutrons generated by 6-18 mv x-ray beams for radiotherapy. *Health Physics*, 80(1), 4–11. <https://doi.org/10.1097/00004032-200101000-00003>
- Faiz, M. K., & John, G. P. (2014). *The physics of radiation therapy*. Wolters Kluwer.
- Fleckenstein, J., Jahnke, L., Lohr, F., Wenz, F., & Hesser, J. (2013). Development of a geant4 based monte carlo algorithm to evaluate the monaco vmat treatment accuracy. *Medical Physics*, 23(1), 33–45. <http://dx.doi.org/10.1016/j.zemedi.2012.08.002>
- Freeman, J. A., & Skapura, D. M. (1991). *Neural networks: Algorithms, applications and programming techniques computation and neural systems*. Addison-Wesley.
- Hamed Abd El-Kader, E. A. (2014). Dosimetry measurements of radiation fields. *Research & Reviews in BioSciences*, 8(8), 302–318.
- IAEA. (2004). *Dosimetry codes of practice and worksheets - International atomic energy agency*.
- Kandlakunta, P., Momin, S., Sloop, A., Zhang, T., & Khan, R. (2019). Characterizing a geant4 monte carlo model of a multileaf collimator for a truebeam, c linear accelerator. *Physica Medica*, 59, 1–12. <https://doi.org/10.1016/j.ejmp.2019.02.008>
- Knoll, G. F. (2010). *Radiation detection and measurement* (4th ed.). Wiley.
- Kumar, A., & Pavel, T. (2015). A new approach to nuclear reactor design optimization using genetic algorithms and regression analysis. *Annals of Nuclear Energy*, 85, 27–35. <https://doi.org/10.1016/j.anucene.2015.04.028>
- Langdon, W. B., & Poli, R. (2002). *Foundations of genetic programming*. Springer-Verlag.
- Li, G., Zheng, H., Sun, G., & Wu, Y. (2011). Photon energy spectrum reconstruction based on monte carlo and measured percentage depth dose in accurate radiotherapy. *Progress in Nuclear Science and Technology*, 2, 160–164. <https://doi.org/10.15669/pnst.2.160>
- Medhat, M. E. (2012). Artificial intelligence methods applied for quantitative analysis of natural radioactive sources. *Annals of Nuclear Energy*, 45, 73–79. <https://doi.org/10.1016/j.anucene.2012.02.013>
- Mesbahi, A., Reilly, A. J., & Thwaites, D. I. (2006). Development and commissioning of a monte carlo photon beam model for varian clinic 2100ex linear accelerator. *Applied Radiation and Isotopes*, 64(6), 656–662. <https://doi.org/10.1016/j.apradiso.2005.12.012>
- Mijnheer, B. J., Battermann, J. J., & Wambersie, A. (1987). What degree of accuracy is required and can be achieved in photon and neutron therapy? *Radiotherapy and Oncology: Journal of the European Society for Therapeutic Radiology and Oncology*, 8(3), 237–252. [https://doi.org/10.1016/S0167-8140\(87\)80247-5](https://doi.org/10.1016/S0167-8140(87)80247-5)
- Pal, S., Muthukrishnan, G., Ravishankar, R., Sharma, R., & Ghose, A. (2002). Estimation of percentage depth dose distributions for therapeutic machines. *Radiation Physics and Chemistry*, 65(6), 589–594. [https://doi.org/10.1016/S0969-806X\(02\)00270-0](https://doi.org/10.1016/S0969-806X(02)00270-0)
- Panettieri, V., Barsoum, P., Westermark, M., Brualla, L., & Lax, I. (2009). Aaa and pbc calculation accuracy in the surface build-up region in tangential beam treatments. phantom and breast case study with the monte carlo code penelope. *Radiotherapy and Oncology*, 93(1), 94–101. <https://doi.org/10.1016/j.radonc.2009.05.010>
- Pilato, V., Tola, F., Martinez, J. M., & Huver, M. (1999). Application of neural networks to quantitative spectrometry analysis. *Nuclear Instruments and Methods in Physics Research*, 422(1-3), 423–427. [https://doi.org/10.1016/S0168-9002\(98\)01110-3](https://doi.org/10.1016/S0168-9002(98)01110-3)
- Pinheiro, V. H. C., & Schirru, R. (2018). Genetic programming applied to the identification of accidents of a pwr nuclear power plant. *Annals of Nuclear Energy*, 124, 335–341. <https://doi.org/10.1016/j.anucene.2018.09.039>

- Podgorsak, E. (2006). *Radiation oncology physics: A handbook for teachers and students, international atomic energy agency* (Vol. 33). International Atomic Energy Agency.
- Pozzi, S., & Segovia, J. (2000). Evaluation of genetic programming and neural networks techniques for nuclear material identification. *Proceedings of the 2nd Annual Conference on Genetic and Evolutionary Computation*, 2, 590–596.
- Price, W. J. (1964). *Nuclear radiation detection* (2nd ed.). McGraw-Hill.
- Ramirez, J. L. V., Chen, F., Nicolucci, P., & Baffa, O. (2011). Dosimetry of small radiation field in inhomogeneous medium using alanine/epr minidosimeters and penelope monte carlo simulation. *Radiation Measurements*, 46(9), 941–944. <https://doi.org/10.1016/j.radmeas.2011.06.008>
- Reza, M., Islam, M., Rahman, M., Shamsuzzaman, M., Rahman, M., & Khan, H. R. (2018). Calibration of therapy level ionization chamber at 60co teletherapy beam used for radiation therapy, international letters of chemistry, physics and astronomy. *International Letters of Chemistry, Physics and Astronomy*, 79, 1–8. <https://doi.org/10.18052/www.scipress.com/ILCPA.79.1>
- Santos, J. A. L., Silva, E. R., Ferreira, T. A. E., & Villela, E. C. (2012). Unfolding neutron spectra obtained from bs tld system using genetic algorithm. *Applied Radiation and Isotopes*, 71, 81–86. <https://doi.org/10.1016/j.apradiso.2012.06.031>
- Sawakuchi, G. O., Mirkovic, D., Perles, L. A., Sahoo, N., Zhu, X. R., Ciangaru, G., Suzuki, K., Gillin, M. T., Mohan, R., & Titt, U. (2010). An mcnp model of a discrete spot scanning proton beam therapy nozzle. *Medical Physics*, 37(9), 4960–4970. <https://doi.org/10.1118/1.3476458>
- Vega-Carrillo, H. R., Hernández-Dávila, V. M., Manzanares-Acuña, E., Sánchez, G. A. M., de la Torre, M. P. I., Barquero, R., Palacios, F., Villaflañe, R. M., Arteaga, T. A., & Rodríguez, J. M. O. (2006). Neutron spectrometry using artificial neural networks. *Radiation Measurements*, 41(4), 425–431. <https://doi.org/10.1016/j.radmeas.2005.10.003>
- Welcome to gplearn's documentation, — gplearn 0.4.1 documentation. (2019). Ed. Trevor Stephens. <https://gplearn.readthedocs.io/en/stable/>
- Wood, R. G. (1974). *Computers in radiotherapy*. Ed. Butterworths.
- Wu, X., & Zhu, Y. (2000). A neural network regression model for relative dose computation. *Physics in Medicine and Biology*, 45(4), 913–922.
- Yoshida, E., Shizuma, K., Endo, S., & Oka, T. (2002). Application of neural networks for the analysis of gamma-ray spectra measured with a ge spectrometer. *Nuclear Instruments and Methods in Physics Research*, 484(1-3), 557–563. [https://doi.org/10.1016/S0168-9002\(01\)01962-3](https://doi.org/10.1016/S0168-9002(01)01962-3)
- Zhang, H., Johnson, E. L., & Zwicker, R. D. (2006). Dosimetric validation of the mcnp model for radiotherapy studies of megavoltage grid radiotherapy. *International Journal of Radiation Oncology Biology Physics*, 66(5), 1576–1583. <https://doi.org/10.1016/j.ijrobp.2006.08.059>